

Modeling of anisotropic hardening and grain size effects based on advanced numerical methods and crystal plasticity

B. BERISHA¹⁾, S. HIRSIGER²⁾, H. HIPPE²⁾, P. HORA²⁾,
A. MARIAUX³⁾, D. LEYVRAZ³⁾, C. BEZENÇON³⁾

¹⁾*Inspire AG, Institute of Virtual Manufacturing (inspire-ivp), Tannenstrasse 3, 8092 Zurich, Switzerland, e-mail: e-mail: berisha@inspire.ethz.ch*

²⁾*ETH Zurich, Institute of Virtual Manufacturing (ivp), Tannenstrasse 3, 8092 Zurich, Switzerland*

³⁾*Novelis Switzerland SA, Route des Laminoirs 15, 3960 Sierre, Switzerland*

MODELING OF ANISOTROPIC BEHAVIOR as well as hardening behavior based on micromechanical quantities in combination with a spectral solver is the focus of this study. A deep drawing steel as well as two different aluminum alloys are investigated. Prediction capabilities of the proposed modeling strategy are discussed and the benefits of the micromechanical model are highlighted. Further, a comparison of the crystal plasticity (CP) results with the well established macroscopic model YLD2000-2d underlines the importance of the CP as a complementary modeling technique to the macroscopic modeling. Both models – the microscopic as well as the macroscopic – are validated on experimental data mainly gained from uniaxial and biaxial tests. In the second part of this study, strong inhomogeneous microstructures are investigated from a modeling point of view. For this purpose, a Hall–Petch phenomenological model is implemented in the CP open-source code DAMASK to take the grain size effects into account. Appropriate combinations of the grain sizes in a bimodal microstructure are presented in order to increase the strength as well as ductility of a generic aluminum alloy. The proposed numerical strategy of coupling the CP and efficient FFT-based spectral solver supports the development of new materials in an optimal way.

Key words: bimodal microstructures, anisotropic hardening, crystal plasticity, Fast Fourier Transform, grain size effects.

Copyright © 2019 by IPPT PAN, Warszawa

1. Introduction

THE QUALITY OF THE OPTIMIZATION OF METAL FORMING PROCESSES strongly depends on material models used. In addition, determination of the model parameters is commonly the most time consuming part and can be very expensive, due to the needed experimental data. As the models are getting more and more complex, the number and complexity of the required experiments is increasing continuously as well. In the sheet metal forming context, these requirements are even more pronounced, because of the anisotropic behavior of the

sheet materials. In general, tensile tests in at least three directions, biaxial tests and tension-compression or shear-reverse shear experiments are performed to determine the parameters of the macroscopic models, e.g. the HAH model [1]. Hence, determination of the macroscopic model parameters based on virtual experiments is a very promising strategy to overcome these difficulties and to reduce the number of real experiments to a minimum. For this purpose, in the framework of this study, following topics are covered:

- Prediction of the anisotropic behavior (yield locus) based on crystal plasticity simulations
- Investigation of the influence of the grain size on the hardening behavior on bimodal microstructures.

Macroscopic yield loci are widely used in the sheet metal forming community due to their computational efficiency compared to multiscale CP based material modelling. The number of available models is high and their complexity differs greatly and therefore, choosing an appropriate description of the anisotropic behavior of considered material still remains a challenge. An overview of the currently available models is given in [2–4]. Correct modeling of the anisotropic behavior is of crucial importance, because the shape of the yield locus and moreover, the normal on the yield surface, has a direct influence on the strain distribution on a part. As a further aspect the strain distribution strongly influences the failure occurrence as well. For cubic metals like aluminum and steel, symmetry in yielding between tensile and compressive loading is generally assumed. In consequence, the established YLD2000-2d mathematical model presented in [5] is widely used. In general, anisotropic hardening phenomena are described using kinematic-hardening models as proposed e.g. in [6]. An alternative to the kinematic hardening models is proposed in [1].

Materials with bimodal microstructures have gained special attention in the past, because of their high strength and ductility properties. Various models at different length scales, ranging from dislocation based up to analytical ones, have been presented to model grain size effects on hardening and failure behavior [7–9]. A summary of the modeling techniques can be found in [7]. An analytical model to describe hardening and failure behavior of bi-modal nanoaluminum alloys has been presented in [9]. Prediction capabilities of the model were tested on an aluminum alloy manufactured using powder metallurgy techniques. Manufacturing of bimodal microstructures is currently limited to some special processes of powder metallurgy [9–11], friction stir processing [12, 13], high pressure torsion [14]. In general, the base microstructure of bimodal microstructures is generated from a severe plastic deformation process (SPD) like ARB (Accumulative Roll Bonding), ECAP (Equal Channel Angular Pressing) or HPT (High Pressure Torsion). An overview of common SPD processes can be found in [15] and [16].

2. Crystal plasticity model

Computation of the microstructural response of the Representative Volume Elements (RVE) are done with the open source DAMASK kit [17]. DAMASK provides physically based as well as physically motivated phenomenological crystal plasticity models. The physically based models have in general a large number of material parameters, which make them difficult to be used in real case studies. For this purpose, the classical physically motivated phenomenological model has been applied in the present study. The crystal plasticity model discussed in this study is formulated in a finite strain framework and the kinematics of deformation are described in three different configurations: reference, intermediate and current configuration. The multiplicative decomposition of the deformation gradient $\mathbf{F} = \mathbf{F}_e \mathbf{F}_p$ enables one computation of quantities in the intermediate configuration in which for example the second Piola–Kirchhoff stress \mathbf{S} is defined. The CP model is explained below and detailed explanations can be found e.g. in [18] and [19]. If only plastic deformation due to dislocation slip is considered, the plastic part of the velocity gradient can be given by

$$(2.1) \quad \mathbf{L}_p = \dot{\mathbf{F}}_p \mathbf{F}_p^{-1} = \sum_{\alpha=1}^{N_{slip}} \dot{\gamma}^\alpha (\mathbf{m}^\alpha \otimes \mathbf{n}^\alpha).$$

This relationship returns the shear strain rate $\dot{\gamma}^\alpha$ on a direction \mathbf{m}^α of the slip system α described by its normal \mathbf{n}^α . The evolution equation for $\dot{\gamma}^\alpha$ is given by

$$(2.2) \quad \dot{\gamma}^\alpha = \dot{\gamma}_0 \left| \frac{\tau^\alpha}{\tau_c^\alpha} \right|^{\frac{1}{n_{slip}}} \cdot \text{sgn}(\tau^\alpha),$$

where τ^α and τ_c^α are the resolved shear stress and the critical shear stress, respectively. The relationship between the second Piola–Kirchhoff stress tensor and the resolved shear stress is given in Eq. (2.3)

$$(2.3) \quad \tau^\alpha = \mathbf{F}_e^T \mathbf{F}_e \mathbf{S} : (\mathbf{m}^\alpha \otimes \mathbf{n}^\alpha)$$

with $\mathbf{F}_e^T \mathbf{F}_e \mathbf{S}$ defining the Mandel stress tensor and \mathbf{S} the second Piola–Kirchhoff stress tensor

$$(2.4) \quad \mathbf{S} = \frac{1}{2} \mathbb{C} : (\mathbf{F}_e^T \mathbf{F}_e - \mathbf{I}),$$

where \mathbb{C} is the fourth order elasticity tensor. The most popular evolution equation for the critical shear stress is given in (2.5)

$$(2.5) \quad \dot{\tau}_c^\alpha = \sum_{\beta=1} h^{\alpha\beta} |\dot{\gamma}^\beta|$$

with the interaction matrix $h^{\alpha\beta}$ between the slip systems α and β

$$(2.6) \quad h^{\alpha\beta} = q^{\alpha\beta} \left[h_0 \left(1 - \frac{\tau_c^\beta}{\tau_{sat}^\alpha} \right)^a \right].$$

In general, $q^{\alpha\beta}$ is set to 1, if α and β are coplanar. Otherwise, $q^{\alpha\beta} = 1.4$.

In the framework of this study, the investigations of the grain size effects on hardening behavior is based on a similar model as presented in [20]. This model has been implemented in DAMASK [21]. Main equations are given in (2.7) and (2.8)

$$(2.7) \quad \tilde{\tau}_{c,0}^\alpha = \tau_{c,0}^\alpha + k_1 \frac{1}{\sqrt{d}},$$

$$(2.8) \quad \tilde{\tau}_{sat}^\alpha = \tau_{sat}^\alpha + k_2 \frac{1}{\sqrt{d}},$$

where d is the grain size and k_1, k_2 are material constants. The influence of the grain size on the hardening behavior of a generic material is discussed in Section 5.

3. Material modeling based on crystal plasticity and a FFT-spectral solver

In the context of micro mechanical material design usually a Representative Volume Element (RVE) is considered. The spectral solver based on FFT (Fast Fourier Transform) is an alternative to the classical FEM solvers, if periodic boundary conditions are admissible. The basic idea of the FFT-method is to transform the partial differential equations into the frequency domain and to solve the resulting algebraic system of equations therein. It is worth to mention that, in contrast to FEM, the equilibrium equation is fulfilled at each grid point. For the sake of completeness a short summary of the method is given below. For more details see [22].

The static equilibrium can be described using e.g. the first Piola-Kirchhoff stress tensor

$$(3.1) \quad \text{Div} \mathbf{P} = \mathbf{0}.$$

The Fourier transform $\hat{\mathbf{F}}(\mathbf{K}) = \mathcal{F}\{\mathbf{F}(\mathbf{X})\}$ of the deformation gradient $\mathbf{F}(\mathbf{X})$ can then be given as

$$(3.2) \quad \hat{\mathbf{F}}(\mathbf{K}) = \begin{cases} -\hat{\mathbb{G}}(\mathbf{K})\hat{\boldsymbol{\tau}}(\mathbf{K}), & \mathbf{K} \neq \mathbf{0}, \\ \bar{\mathbf{F}}\delta(\mathbf{K}), & \mathbf{K} = \mathbf{0}, \end{cases}$$

where $\hat{\mathbb{G}}$ is the so called "Gamma Operator" given in [22], \mathbf{K} are coordinates of the spectral space, δ is the Dirac-Delta and $\bar{\mathbf{F}}$ the averaged deformation gradient; $\boldsymbol{\tau}$ is the so called polarization field and is defined as $\boldsymbol{\tau}(\mathbf{X}) = \mathbf{P}(\mathbf{X}) - \mathbb{A}\mathbf{F}(\mathbf{X})$, with \mathbb{A} representing the stiffness of a linear comparison material.

Similar to the nonlinear FEM method an iterative scheme is used to solve the resulting nonlinear system of equations. For this purpose, DAMASK provides several algorithms and a comparison of the methods is discussed in [23]. In the context of the well known *Fix Point Method* the equations at the current iteration can be given as

$$(3.3) \quad \mathbf{F}^{(n+1)}(\mathbf{X}) = \mathbf{F}^{(n)}(\mathbf{X}) + \mathcal{F}^{-1} \begin{cases} -\hat{\mathbb{G}}(\mathbf{K})\hat{\mathbf{P}}^{(n)}(\mathbf{K}), & \mathbf{K} \neq \mathbf{0}, \\ (\bar{\mathbf{F}}^{(BC,n+1)} - \bar{\mathbf{F}}^{(n)})\delta(\mathbf{K}), & \mathbf{K} = \mathbf{0}, \end{cases}$$

with respect to the prescribed boundary conditions

$$(3.4) \quad \bar{\mathbf{F}}^{(BC,n+1)} = \bar{\mathbf{F}}^{(0)} + \dot{\bar{\mathbf{F}}}^{(BC)}\Delta t + \left\{ \frac{\partial \mathbf{F}}{\partial \mathbf{P}} \right\}^{(n)} (\bar{\mathbf{P}}^{(BC)} - \bar{\mathbf{P}}^{(n)})$$

where the superscript (0) represents quantities at the beginning of the increment, (BC) stands for boundary conditions and Δt is the time increment. Averaged quantities are denoted by $(\bar{\quad})$ and therefore, $\frac{\partial \mathbf{F}}{\partial \mathbf{P}}$ represents the average compliance.

3.1. RVE-modeling in the framework of a FFT-solver

Various microstructural quantities like shape and orientation of the grains, the crystal system and other microstructure features have an influence on the anisotropic behavior of metals, see e.g. [24]. In the framework of this study the anisotropic behavior of the investigated materials is characterized by the orientations of the grains, the texture. The well known methods based on X-ray diffractometry enable one to measure the pole figures and thereafter compute the ODF (Orientation Distribution Function). The ODF can be used directly as an input for the RVE. However, the number of measured orientations is in general too big and cannot be used directly for the numerical simulations, because of the resulting high computational cost. The number of orientations of an ODF can be reduced using various algorithms, e.g. [25]. It is shown in [21] that the reduction of the orientations can have a significant influence on the resulting behavior of the considered microstructure. If the reduced ODF contains in addition to the representative orientations some other components with a high intensity, the model response is not accurate enough. For the investigated materials measured as well as reduced ODFs are shown in Figs. 2 and 3, for DC05 and AA6016-T4, respectively. A RVE discretization by 16^3 for both materials has been used,

whereas for the bimodal microstructure the number of FFT points is set to 128^3 , because of the very small grains ($\approx 1 \mu m$) considered in the microstructure. In [26, 27] 25 and 50 representative orientations have been considered, respectively. In contrast to that, in the current study $1.6 \cdot 10^4$ orientations has been defined to model the bimodal microstructure. The number of the FFT points corresponds with the given discretization: 16^3 for the homogeneous material and 128^3 for the bimodal microstructure. This means that for 50 grains ≈ 80 FFT points per grain were considered for the homogeneous microstructure. For the bimodal microstructure $\approx 1.6 \cdot 10^4$ fine grains with a volume partition of 85% and therefore ≈ 110 FFT points per grain were considered. For the coarse grains inside the bimodal microstructure the number of FFT-points is much higher ($\approx 3 \cdot 10^4$), due to the uniform distribution of the FFT points inside the RVE.

4. Calculation of yield locus based on crystal plasticity

4.1. Calculation of yield loci without pre-straining of the material

A common possibility to describe the anisotropic behavior of a material is the description of its yielding behavior in the σ_x - σ_y stress space. For this purpose, several stress ratios have been defined and applied as boundary conditions to the RVE to detect the yielding point and to compare it with the well established macroscopic yield locus model Yld2000-2d [5]. The results of the CP-simulations and the macroscopic model are shown in Fig. 1a and 1b, whereas the fitted model parameters are given in Tables 2 and 3. Both figures show that yield loci based on CP simulations are able to represent the anisotropic behavior of the investigated materials with a sufficient accuracy. The CP based prediction of

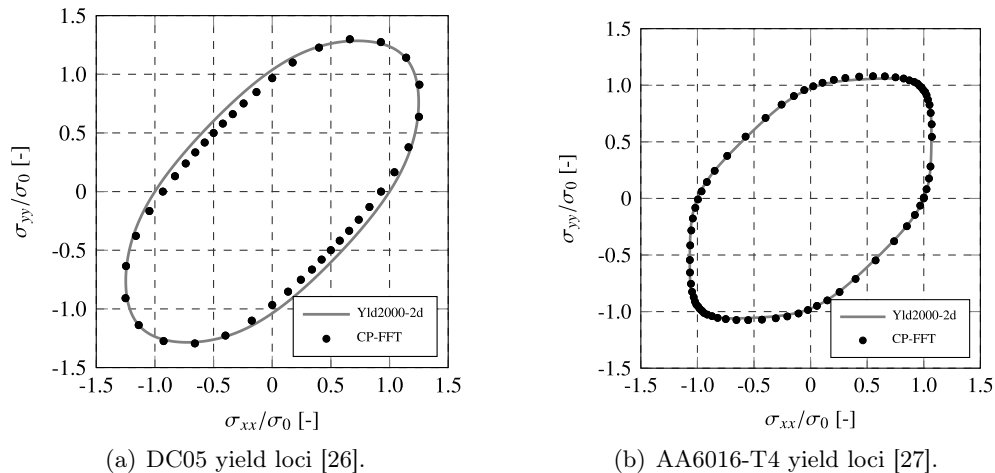


FIG. 1. Macroscopic yield loci vs. CP-FFT prediction.

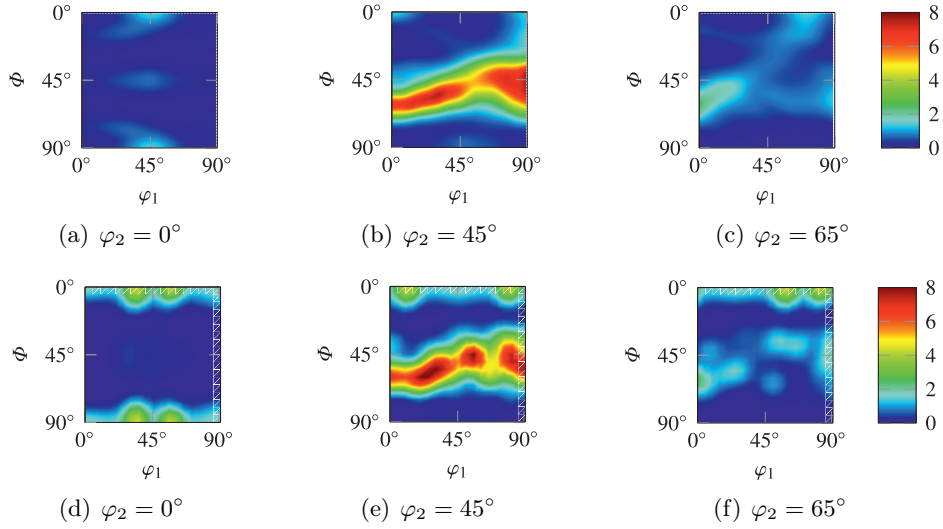


FIG. 2. Measured (top row) and reduced (bottom row) ODF of DC05 [26].

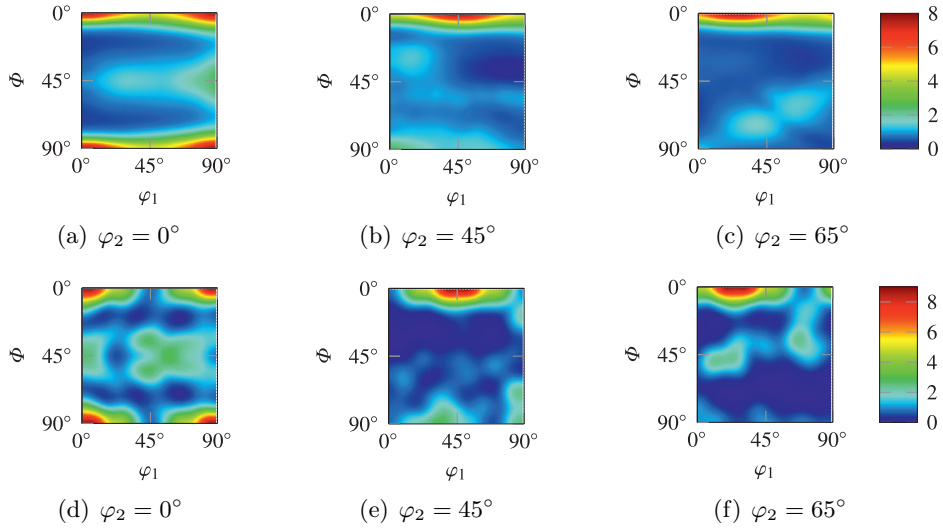


FIG. 3. Measured (top row) and reduced (bottom row) ODF of AA6016-T4 [27].

yielding compared to the macroscopic model YLD2000-2d can be summarized as follows:

- DCO5: a negligible small deviation in the fourth quadrant has been observed. Otherwise, practically no difference between the models.
- AA6016: an excellent agreement between the models is obtained.

Table 1. Normalized material properties.

Material	σ_0/σ_0	σ_{45}/σ_0	σ_{90}/σ_0	σ_b/σ_0	r_0	r_{45}	r_{90}	r_b
DC05	1.00	1.05	1.04	1.14	2.00	1.47	2.52	0.85
AA6016-T4	1.00	0.96	0.98	0.99	0.69	0.50	0.67	1.00

Table 2. Fitted hardening parameters for the CP model for the materials DC05 and AA6016-T4 based on the ODF and yield curves given in [28] and [29], respectively.

Material	$\tau_{c,0}$	τ_{sat}	h_0	a	n
DC05	58.00 MPa	151.0 MPa	900.0 MPa	2.1	60
AA6016-T4	42.85 MPa	120.8 MPa	503.3 MPa	1.3	50

Table 3. Fitted Yld2000-2d parameters for DC05 [28] and for AA6016-T4 [29]. Tensile tests in 0, 45 and 90° to rolling direction and an equibiaxial test were performed to fit the Yld200-2d parameters.

Material	a	α_1	α_2	α_3	α_4	α_5	α_6	α_7	α_8
DC05	6	1.084	0.982	0.846	0.881	0.908	0.836	0.972	0.975
AA6016-T4	8	0.947	1.107	0.961	1.032	1.021	1.013	0.967	1.153

4.2. Calculation of yield loci for the pre-strained material

Real forming processes contain in general nonlinear strain paths. The predictive capabilities of the presented CP-model are tested on the DC05 steel grade, which was first prestrained in rolling direction up to $\epsilon_{11} = 0.15$ followed by a transverse uniaxial or an equibiaxial deformation. The responses of several models are shown in Fig. 4. The CP-model predicts both experimental points with a sufficient accuracy. In addition, a slightly anisotropic hardening of the CP-prediction could be observed, see for further details [26]. The classical Taylor model seems to predict the yield point in transverse direction pretty well. However, in the equibiaxial region the deviation is very high. Even the HAH model [1] does not show the desirable predictive capabilities. Nevertheless, several extensions of the first version of the distortional hardening model HAH, presented in [1], have been recently published in [30] and [31], which could show a more appropriate behavior of the model in the transverse direction. A comparison of the experimental effort between the CP-modeling and the macroscopic modeling e.g. the HAH model can be summarized as follows:

- For the CP model only the ODF and the uniaxial hardening curve is required to determine the material parameters.

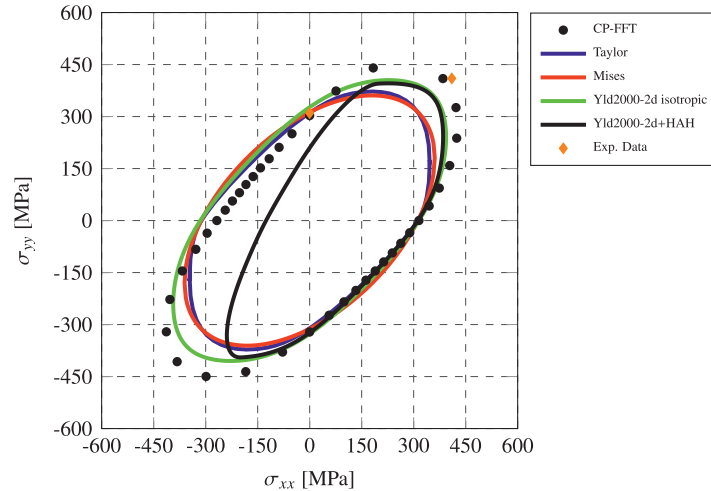


FIG. 4. Comparison of the CP-prediction and various macroscopic models for the prestrained material of $\varepsilon_{11} = 0.15$ in rolling direction [26].

- For the macroscopic HAH model following experiments are necessary
 - Tensile tests in three different directions (0° , 45° and 90° to rolling direction).
 - One equi-biaxial test to determine the biaxial yield stress and one compression test to determine the Lankford-parameter (R-Value).
 - At least one test with load reversal e.g. shear-reverse shear, if for example the Bauschinger effect has to be modeled.

5. Bimodal microstructures – grain size effects

Depending on the defined requirements for the properties of a material e.g. high yield stress, high strength or high ductility and fracture strain etc., several mechanical, thermal and alloying strategies are applied. The big challenge is to combine e.g. high strength and ductility of a material. Bimodal microstructures show promising properties in this context. In general, bimodal microstructures consist of a matrix in the ultrafine grained range – ufg¹, responsible for high strength, and coarser grains, responsible for high ductility. Several work have been published in this context, to name some few, representative publications are shortly discussed below.

A nanostructured hierarchical AA7075 aluminum alloy approximating a tensile strength of 1 GPa has been presented in [32]. However, the high strength alloy

¹ufg-range: grainsize between 100 nm and 1 μm .

showed a uniform elongation of only $\approx 5\%$. A summary of various heterogeneous microstructures with specific mechanical properties is presented in [16]. A bimodal stainless steel showing high strength and ductility is presented in [33]; [34] proposed a thermomechanical strategy to manufacture copper with a bimodal microstructure. The achieved material properties result in very high strengths and ductility. In [35] the mechanical properties and the numerical modeling of heterogeneous (bimodal, gradient etc.) nanostructured single phase materials have been discussed. A material model for FCC ultrafine-grains/nanocrystalline grains has been presented in [36]. Grain boundary segregation of nanocrystalline binary aluminum alloys has been investigated in [37] based on MD (Molecular Dynamics) simulations. Strain rate sensitivity of bimodal Al-laminates manufactured via accumulative roll bonding (ARB) has been discussed in [38]. The alternating layers were defined from a commercial purity aluminum (Al99.5) and a high purity aluminum (Al99.999). A summary of the mechanical behavior of nano-grain Cu and Cu-based alloys as well as bimodal microstructures is presented in [39]. Rolling technologies for producing ultrafine-grains/nanograins are summarized in [40].

In addition to the advances in manufacturing technologies for the production of ufg and bimodal microstructures, numerical methods enabling an efficient modeling of the microstructure have been developed as well. Modeling of the plastic behavior of metals based on crystal plasticity theory is a well-established methodology. However, in the framework of CPFEM, the computation time is very high and therefore, the computations are restricted to simplified microstructures as well as simple polycrystal models. In the presented work, an efficient coupling of a physically motivated phenomenological crystal plasticity model – including an implementation of grain size effects – and the FFT-spectral solver of the code DAMASK [17] is proposed.

In the following, hardening behavior of uniaxial as well as model predictions for biaxial loading cases are discussed. In this context, Eqs. (2.7) and (2.8) have to be considered. It is worth to mention that manufacturing of bimodal aluminum remains a challenge. However, based on available experimental data of homogeneous microstructures, several model predictions are discussed and the potential of bimodal microstructures is highlighted.

5.1. Determination of the material parameters

The additional parameters k_1 and k_2 in Eqs. (2.7) and (2.8) of the material model have been fitted on measured hardening curves for two different grain sizes: $12\ \mu\text{m}$ and $29\ \mu\text{m}$, see Fig. 5(a) and 5(b). The corresponding ODFs are shown in Fig. 6. Both microstructures show practically the same ODF. A specific thermal treatment strategy has been applied to exclude the influence of the cold work,

which is of crucial importance when the influence of the grain size on hardening is investigated.

Various optimization strategies can be applied to determine the unknown parameters of the explained model. The mathematical optimization has been covered on a cluster, to enable parallel computing and thus reducing the computational time significantly. In this context, a quadratic adaptive response surface

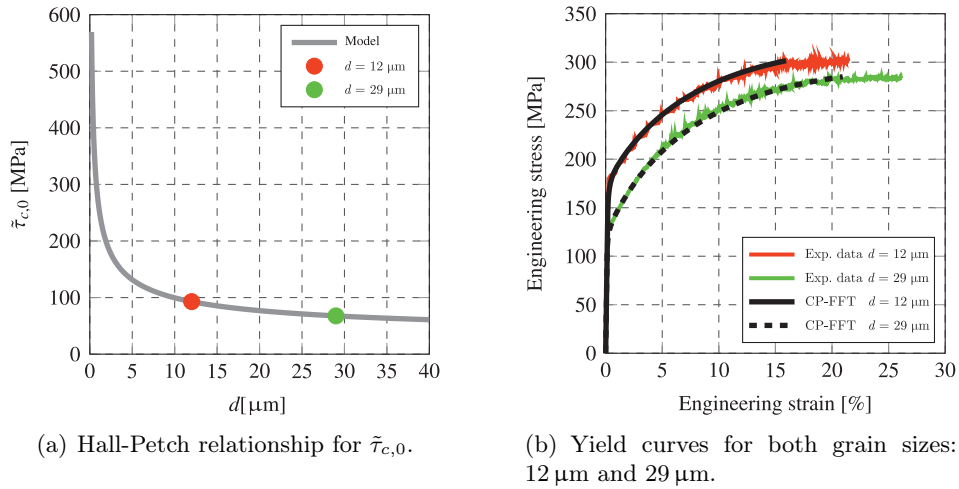


FIG. 5. Grain size effect in AA5356.

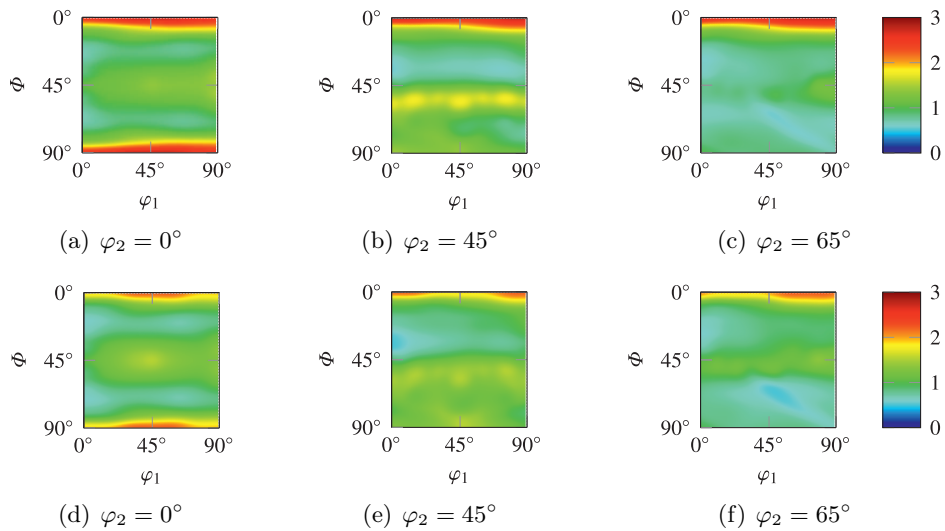


FIG. 6. The ODFs of the AA5356 alloy: grain size 12 μm (top) and 29 μm (bottom).

methodology with a D-optimal sampling technique has been applied. 32 parallel simulations were performed to minimize the objective function given below

$$(5.1) \quad f = \|\mathbf{y}_{model} - \mathbf{y}_{exp}^{fine}\|^2 + \|\mathbf{y}_{model} - \mathbf{y}_{exp}^{coarse}\|^2,$$

where $\mathbf{y}_{exp}^{coarse}$ (grain size $d = 29 \mu\text{m}$) and \mathbf{y}_{exp}^{fine} (grain size $d = 12 \mu\text{m}$) represent the measured hardening behavior of the coarse and fine grain material, respectively. Table 4 shows the fitted model parameters for the aluminum alloy AA5356.

Table 4. Hardening parameters for the CP model with grain size effects.

Material	$\tau_{c,0}$	τ_{sat}	h_0	k_1	k_2	a	n
AA5356	12.35 MPa	135.05 MPa	612.39 MPa	19.13 mm ^{1/2}	20.97 mm ^{1/2}	2.0	50

The quality of the fit is shown in Figure 5(b). It can be highlighted that the proposed CP-model is able to represent the hardening behavior simultaneously for both grain sizes. Further, there is no significant difference in the hardening slope of the considered curves and therefore, the grain size parameters k_1 and k_2 have similar values.

5.2. Prediction of the hardening behavior of a bimodal microstructure

The influence of the grain size on hardening behavior is well studied experimentally as well as from a mathematical modeling point of view [16, 20, 41–43]. The tendency is obvious: if the grain size decreases the yield stress increases. However, the well known disadvantage still remains, namely, the uniform elongation decreases significantly. For the aluminum alloy AA5356 the influence of the grain size on the yield stress is shown in Fig. 7(b). The yield curves of the generic bimodal structures with a reasonable hardening rate and high uniform elongation show a very promising and interesting behavior. A selected RVE (Representative Volume Element) of the bimodal microstructure is shown in Fig. 7(a). The volume fraction of the coarse grains is $\approx 15\%$.

5.3. Determination of yield locus for the generic bimodal microstructure

In addition to the hardening behavior in the uniaxial tension, the biaxial hardening behavior is also of crucial importance for characterizing the forming properties of a material. For this purpose, the yield locus for the presented bimodal microstructure has been computed, see Fig. 8. In contrast to the measured ODF for AA6016 and DC05, for the bimodal microstructure no measurements are currently available, because the real material does not yet exist. The ODF

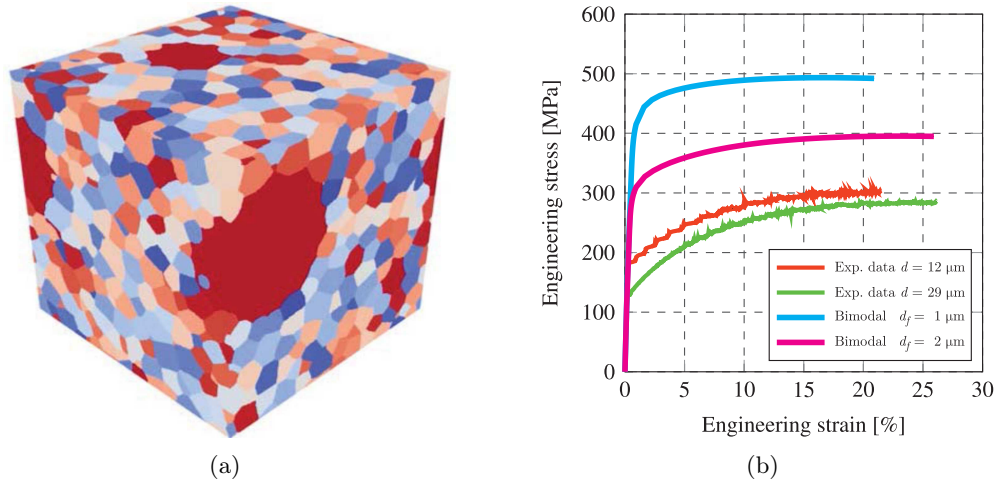


FIG. 7. Selected bimodal RVE and numerical predictions of strain hardening. (a) RVE of a bimodal microstructure: $d_f \approx 2.5 \mu\text{m}$ (fine grain) and $d_c \approx 20 \mu\text{m}$ (coarse grain); (b) predicted yield curves of representative bimodal microstructures and measured yield curves of AA5356 with a homogeneous microstructure – which were used to calibrate the CP-model (see Fig. 5(b)).

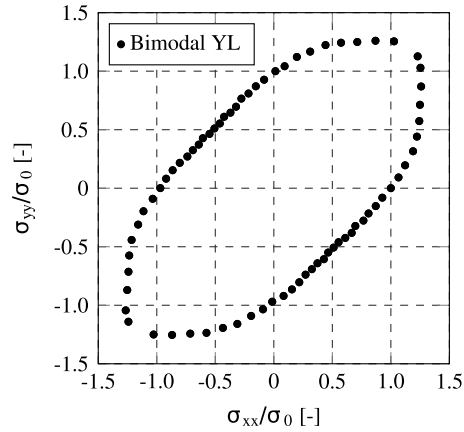


FIG. 8. Predicted yield locus of the AA5356 alloy with a bimodal microstructure.

has been generated using the open-source MTEX toolbox [44]. The main components of the fine grains are chosen to be Brass components, for the coarse grains Cube components have been defined. A scatter of 10° of the orientations has been included, in order to avoid too sharp/artificial grain orientations.

It can be highlighted that the equibiaxial point is shifted to higher stresses, which leads to a significant benefit compared to the classical anisotropic behavior

of the aluminum alloys as shown e.g. in Fig. 1(b) for the well established alloy AA6016-T4. From a modeling point of view, bimodal microstructures seem to have very promising forming properties also in multiaxial loading cases.

6. Conclusions and outlook

It can be concluded that an efficient coupling of crystal plasticity models and the FFT-spectral solver leads to a significant reduction of the amount of real experiments needed to calibrate macroscopic models. Further, due to the time efficient spectral solver used in the computation of the RVE models, detailed modeling of the microstructure is possible. From a modeling point of view it was demonstrated that bimodal microstructures have the potential to achieve high strength and ductility as well as a more appropriate anisotropic behavior for metal forming. Manufacturing of bimodal Al-alloys on the lab-scale is the subject of the ongoing work. Those experiments will enable a validation of the CP-models regarding anisotropic hardening as well as prediction of the yield curve.

Acknowledgements

The authors would like to express sincere gratitude to Innosuisse – Swiss Innovation Agency for the financial support of this study (Project No.: 26515.1 PFIW-IW).

References

1. F. BARLAT, J.J. GRACIO, M.-G. LEE, E.F. RAUCH, G. VINCZE, *An alternative to kinematic hardening in classical plasticity*, International Journal of Plasticity, **27**, 9, 1309–1327, 2011, DOI: 10.1016/j.ijplas.2011.03.003.
2. D. BANABIC, H.-J. BUNGE, K. PÖHLANDT, A.E. TEKKAYA, *Formability of Metallic Materials, Engineering Materials*, Springer, Berlin, Heidelberg, 2000, DOI: 10.1007/978-3-662-04013-3.
3. D. BANABIC, *Sheet Metal Forming Processes*, Springer, Berlin, Heidelberg, 2010, DOI: 10.1007/978-3-540-88113-1.
4. O. CAZACU, B. REVIL-BAUDARD, N. CHANDOLA, *Plasticity-damage couplings: from single crystal to polycrystalline materials*, 1st ed., Vol. 253 of Solid Mechanics and Its Applications, Springer International Publishing, Cham, 2019, DOI: 10.1007/978-3-319-92922-4.
5. F. BARLAT, J. BREM, J. YOON, K. CHUNG, R. DICK, D. LEGE, F. POURBOGHRAI, S.-H. CHOI, E. CHU, *Plane stress yield function for aluminum alloy sheets – Part 1: theory*, International Journal of Plasticity, **19**, 9, 1297–1319, 2003, DOI: 10.1016/S0749-6419(02)00019-0.

6. J. CHABOCHE, *A review of some plasticity and viscoplasticity constitutive theories*, International Journal of Plasticity, **24**, 10, 1642–1693, 2008, DOI: 10.1016/j.ijplas.2008.03.009.
7. L. ZHU, J. LU, *Modelling the plastic deformation of nanostructured metals with bimodal grain size distribution*, International Journal of Plasticity, **30–31**, 166–184, 2012, DOI: 10.1016/j.ijplas.2011.10.003.
8. M. SHAKOORI OSKOOIE, H. ASGHARZADEH, H. KIM, *Microstructure, plastic deformation and strengthening mechanisms of an Al–Mg–Si alloy with a bimodal grain structure*, Journal of Alloys and Compounds, **632**, 540–548, 2015, DOI: 10.1016/j.jallcom.2015.01.229.
9. J. FERGUSON, M. TABANDEH-KHORSHID, P.K. ROHATGI, K. CHO, C.-S. KIM, *Predicting tensile and compressive mechanical properties of bimodal nano-aluminum alloys*, Scripta Materialia, **72–73**, 13–16, 2014, DOI: 10.1016/j.scriptamat.2013.10.005.
10. A.B. SPIERINGS, K. DAWSON, M. VOEGTLIN, F. PALM, P.J. UGGOWITZER, *Microstructure and mechanical properties of as-processed scandium-modified aluminium using selective laser melting*, CIRP Annals, **65**, 1, 213–216, 2016, DOI: 10.1016/j.cirp.2016.04.057.
11. A.M. ESAWI, N.T. ABOULKHAIR, *Bi-modally structured pure aluminum for enhanced strength and ductility*, Materials & Design, **83**, 493–498, 2015, DOI: 10.1016/j.matdes.2015.06.062.
12. H.S. ARORA, A. AYYAGARI, J. SAINI, K. SELVAM, S. RIYADH, M. POLE, H.S. GREWAL, S. MUKHERJEE, *High tensile ductility and strength in dual-phase bimodal steel through stationary friction stir processing*, Scientific Reports, **9**, 1, Article number: 1972, 2019, DOI: 10.1038/s41598-019-38707-3.
13. W. YANG, H. DING, Y. MU, J. LI, W. ZHANG, *Achieving high strength and ductility in double-sided friction stir processing 7050-T7451 aluminum alloy*, Materials Science and Engineering: A, **707**, 193–198, 2017, DOI: 10.1016/j.msea.2017.09.028.
14. D. ORLOV, Y. TODAKA, M. UMEMOTO, N. TSUJI, *Formation of bimodal grain structures in high purity Al by reversal high pressure torsion*, Scripta Materialia, **64**, 6, 498–501, 2011, DOI: 10.1016/j.scriptamat.2010.11.020.
15. N. TSUJI, Y. SAITO, S.-H. LEE, Y. MINAMINO, *ARB (accumulative roll-bonding) and other new techniques to produce bulk ultrafine grained materials*, Advanced Engineering Materials, **5**, 5, 338–344, 2003, DOI: 10.1002/adem.200310077.
16. A. PINEAU, A. AMINE BENZERGA, T. PARDOEN, *Failure of metals III: fracture and fatigue of nanostructured metallic materials*, Acta Materialia, **107**, 508–544, 2016, DOI: 10.1016/j.actamat.2015.07.049.
17. F. ROTERS, P. EISENLOHR, C. KORDS, D. TJAHHANTO, M. DIEHL, D. RAABE, *DAMASK: the Düsseldorf Advanced Material Simulation Kit for studying crystal plasticity using an FE based or a spectral numerical solver*, Procedia IUTAM, **3**, 3–10, 2012, DOI: 10.1016/j.piutam.2012.03.001.
18. J.W. HUTCHINSON, *Bounds and self-consistent estimates for creep of polycrystalline materials*, Proceedings of the Royal Society A: Mathematical, Physical and Engineering Sciences, **348**, 1652, 101–127, 1976, DOI: 10.1098/rspa.1976.0027.
19. F. ROTERS, P. EISENLOHR, T.R. BIELER, D. RAABE, *Crystal Plasticity Finite Element Methods*, 1st ed., Wiley-VCH Verlag GmbH & Co. KGaA, Weinheim, Germany, 2010, DOI: 10.1002/9783527631483,

20. R.K. VERMA, P. BISWAS, *Crystal plasticity-based modelling of grain size effects in dual phase steel*, Materials Science and Technology **32**, 15, 1553–1558, 2016, DOI: 10.1080/02670836.2015.1131959.
21. S. HIRSIGER, B. BERISHA, P. HORA, *On the prediction of yield loci based on crystal plasticity models and the spectral solver framework*, Journal of Physics: Conference Series, NUMISHEET, **2018**, 1063, 2018.
22. P. EISENLOHR, M. DIEHL, R. LEBENSOHN, F. ROTERS, *A spectral method solution to crystal elasto-viscoplasticity at finite strains*, International Journal of Plasticity, **46**, 37–53, 2013, DOI: 10.1016/j.ijplas.2012.09.012.
23. P. SHANTHRAJ, P. EISENLOHR, M. DIEHL, F. ROTERS, *Numerically robust spectral methods for crystal plasticity simulations of heterogeneous materials*, International Journal of Plasticity, **66**, 31–45, 2015, DOI: 10.1016/j.ijplas.2014.02.006.
24. B. BERISHA, C. RAEMY, C. BECKER, M. GORJI, P. HORA, *Multiscale modeling of failure initiation in a ferritic-pearlitic steel*, Acta Materialia **100**, 191–201, 2015, DOI: 10.1016/j.actamat.2015.08.035.
25. P. EISENLOHR, F. ROTERS, *Selecting a set of discrete orientations for accurate texture reconstruction*, Computational Materials Science, **42**, 4, 670–678, 2008, DOI: 10.1016/j.commatsci.2007.09.015.
26. C. RAEMY, B. BERISHA, P. HORA, *Determination of yield loci based on CP-Models for DC05*, 8th Forming Technology Forum (FTF 2015), pp. 135–138, 2015.
27. S. HIRSIGER, B. BERISHA, P. HORA, *Determination of yield loci based on CP-Models for AA6016*, Internal Report, Institute of Virtual Manufacturing-ETH Zurich, 2017.
28. P. PETERS, *Yield functions taking into account anisotropic hardening effects for an improved virtual representation of deep drawing processes*, Ph.D. thesis, ETH Zuerich, 2015, DOI: 10.3929/ethz-a-010503932.
29. M. GORJI, B. BERISHA, N. MANOPULO, P. HORA, *Effect of through thickness strain distribution on shear fracture hazard and its mitigation by using multilayer aluminum sheets*, Journal of Materials Processing Technology, **232**, 19–33, 2016, DOI: 10.1016/j.jmatprotec.2016.01.014.
30. F. BARLAT, Y. JEONG, J.J. HA, C. TOMÉ, M.G. LEE, W. WEN, *Advances in constitutive modeling of plasticity for forming applications*, Key Engineering Materials, **725**, 3–14, 2016, DOI: 10.4028/www.scientific.net/KEM.725.3.
31. F. BARLAT, *Advanced constitutive modeling for application to sheet forming*, Journal of Physics: Conference Series, **1063**, Article number: 012002, 2018, DOI: 10.1088/1742-6596/1063/1/012002.
32. P.V. LIDDICOAT, X.-Z. LIAO, Y. ZHAO, Y. ZHU, M.Y. MURASHKIN, E.J. LAVERNIA, R.Z. VALIEV, S.P. RINGER, *Nanostructural hierarchy increases the strength of aluminium alloys*, Nature Communications, **1**, 1, Article number: 63, 2010, DOI: 10.1038/ncomms1062.
33. Z. ZHENG, J. LIU, Y. GAO, *Achieving high strength and high ductility in 304 stainless steel through bi-modal microstructure prepared by post-ECAP annealing*, Materials Science and Engineering: A, **680**, 426–432, 2017, DOI: 10.1016/j.msea.2016.11.004.
34. Y. WANG, M. CHEN, F. ZHOU, E. MA, *High tensile ductility in a nanostructured metal*, Nature, **419**, 6910, 912–915, 2002, DOI: 10.1038/nature01133.

35. E. MA, T. ZHU, *Towards strength–ductility synergy through the design of heterogeneous nanostructures in metals*, *Materials Today*, **20**, 6, 323–331, 2017, DOI: 10.1016/j.mattod.2017.02.003.
36. A.S. KHAN, J. LIU, *A deformation mechanism based crystal plasticity model of ultrafine-grained/nanocrystalline FCC polycrystals*, *International Journal of Plasticity*, **86**, 56–69, 2016, DOI: 10.1016/j.ijplas.2016.08.001.
37. R.I. BABICHEVA, S.V. DMITRIEV, L. BAI, Y. ZHANG, S.W. KOK, G. KANG, K. ZHOU, *Effect of grain boundary segregation on the deformation mechanisms and mechanical properties of nanocrystalline binary aluminum alloys*, *Computational Materials Science*, **117**, 445–454, 2016, DOI: 10.1016/j.commatsci.2016.02.013.
38. M. RUPPERT, C. SCHUNK, D. HAUSMANN, H.W. HÖPPEL, M. GÖKEN, *Global and local strain rate sensitivity of bimodal Al-laminates produced by accumulative roll bonding*, *Acta Materialia*, **103**, 643–650, 2016, DOI: 10.1016/j.actamat.2015.11.009.
39. T.J. RUPERT, *The role of complexions in metallic nano-grain stability and deformation*, *Current Opinion in Solid State and Materials Science*, **20**, 5, 257–267, 2016, DOI: 10.1016/j.cossms.2016.05.005.
40. H. YU, K. TIEU, C. LU, *Advanced rolling technologies for producing ultrafine-grain/nanostructured alloys*, *Procedia Engineering*, **81**, 96–101, 2014, DOI: 10.1016/j.proeng.2014.09.133.
41. G. WILDE, *Physical metallurgy of nanocrystalline metals*, [in:] *Physical Metallurgy*, D. Laughlin, K. Hono [eds], pp. 2707–2805, Elsevier Science Ltd., Oxford, 2014, DOI: 10.1016/B978-0-444-53770-6.00026-5.
42. Y. ESTRIN, K. RHEE, R. LAPOVOK, P.F. THOMSON, *Mechanical behavior of alloy AA6111 processed by severe plastic deformation: Modeling and experiment*, *Journal of Engineering Materials and Technology*, **129**, 3, 380–389, 2007, DOI: 10.1115/1.2744396.
43. R. LAPOVOK, I. TIMOKHINA, P. MCKENZIE, R. O'DONNELL, *Processing and properties of ultrafine-grain aluminium alloy 6111 sheet*, *Journal of Materials Processing Technology*, **200**, 1–3, 441–450, 2008, DOI: 10.1016/j.jmatprotec.2007.08.083.
44. F. BACHMANN, R. HIELSCHER, H. SCHAE BEN, *Texture analysis with MTEX – free and open source software toolbox*, *Solid State Phenomena*, **160**, 63–68, 2010, DOI: 10.4028/www.scientific.net/SSP.160.63.

Received November 30, 2018; revised version August 16, 2019.

Published online October 25, 2019.
